ELECTROMOTION 2001
June 19-20, 2001
Bologna - ITALY

A FIELD-CIRCUIT APPROACH TO THE THERMAL MODEL OF WATER COOLED INDUCTION MOTORS

A. Di Gerlando, R. Perini

Dipartimento di Elettrotecnica – Politecnico di Milano, Italy

Abstract - A thermal model of a water cooled induction motor is developed, based on the analytical study of the temperature field within each machine portion and on the consequent synthesis of a lumped parameter thermal network. This field-circuit approach allows to limit the number of network nodes and leads to evaluate both the nodal temperatures and the temperature distribution within each portion, in particular as regards the stator winding.

I. INTRODUCTION

The refinement of the methodologies for the electromagnetic design of the induction motors leads to improve their thermal modelling, in order to increase their performances. Notwithstanding there are examples of FEM numerical solutions of the temperature field, the analytical approach is still surely valid, because it implies an easier implementation, limiting time consuming and computer resources; moreover, it facilitates the integration of the thermal analysis with an iterative optimisation process; finally, it allows a direct approach to the study of the parameter sensitivity of the model.

Usually the thermal analysis is based on a network obtained by subdividing the machine in different parts, in such a way to approximate the temperature field distribution by evaluating suited nodal temperatures.

Nevertheless, the results of this approach are not always completely satisfying, mainly because of uncertain knowledge of the thermal phenomena and because of insufficient radial and axial machine discretisation.

These problems, occurring in air-cooled machines, become crucial in some special motors, i.e. those for submersible pumps, used for pumping water out of deep wells [1], [2], [3]. As for the discretisation, here two aspects are very critical: the high length/diameter ratio (aimed to limit the well diameter) and the presence of water inside the motor (aimed to increase the thermal exchange and to prevent the penetration of the well water).

The machine cooling system is based on the internal water circulation in the axial, vertical direction, along three channels, connecting two mixing chambers, in the top and bottom motor part (fig.1, left: t = top; b = bottom):

- the gap channel, along which a fraction Q_δ of the inner water flow rises and becomes warmer: it shows important thermal exchange factors, thanks to the high speed;
- the stator slot channel, along which the part Q_s of the water flow rises, becoming warmer too, and licking coil active wires and core surfaces;
- the channel of a few circular notches obtained between stator yoke and frame, carrying the descending water flow Q_n: this channel is a thermal exchanger towards the water flow Q_w, that rises along the well.

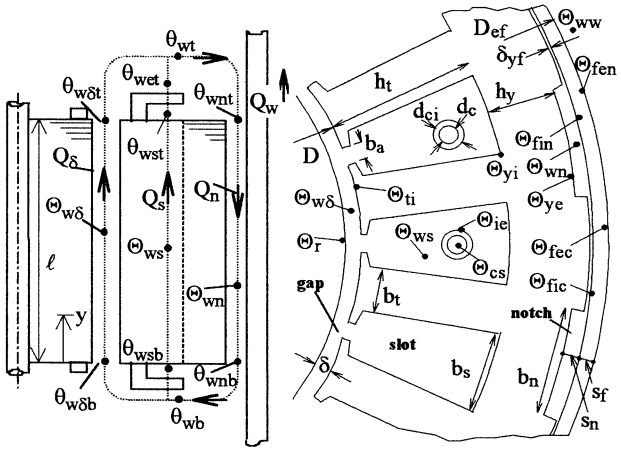

Fig. 1. Induction motor cooling system, with node temperature rises (Θ, θ): left = axial view, with water channel flows Q; right = radial view.

The originality of the proposed approach consists in defining a thermal network in which the number of the thermal nodes (associated with the symbols Θ and θ in fig.1) is not related with a more or less refined discretisation of the field: in fact, the network interconnects a reduced number of circuit elements, each modelling a machine portion "exactly". The qualification of being "exact" is due to the fact that each sub-network follows a separated analytical solution of suited thermal differential equations, for various machine parts: axial cooling channels, stator teeth, stator yoke, coil wires and endwindings.

The solution of the synthesised network gives the nodal temperatures: from these, the thermal field distribution inside each machine portion can be reconstructed.

The paper describes the model development and some simulation results referring to a commercial motor.

II. FIELD-CIRCUIT PROCEDURE TO IDENTIFY THE MOTOR THERMAL SUB-NETWORKS

Referring to fig.1, $\theta_h(y)$ is the axial temperature profile of the h-th motor part, while Θ_h is its average axial value:

$$\Theta_h = \frac{1}{\ell} \cdot \int_0^\ell \theta_h(y) \cdot dy \quad . \tag{1}$$

In order to evaluate the thermal profile $\theta_w(y)$ of the water

flow in each channel, the channel walls are assumed axially isothermal, with temperature rise equal to their average axial value (this hypothesis implies limited errors).

A. Model of the water flow channels

For example, considering the slot channel, the power balance of an axial element of water flow is given by:

$$\left[\sigma_i\cdot(\Theta_{ie}-\theta_{ws})+\sigma_t\cdot(\Theta_t-\theta_{ws})+\right.$$
$$\left.+\sigma_y\cdot(\Theta_{yi}-\theta_{ws})\right]\cdot\alpha_s\cdot p_s\cdot dy = c\cdot\rho\cdot Q_s\cdot d\theta_{ws}\,, \qquad (2)$$

with: $\theta_{ws}(y)$ slot water flow temperature rise profile; Θ_{ie}, Θ_t, Θ_{yi} axial average values of wire insulation surface, teeth walls and yoke internal walls respectively; p_s total wet slot perimeter; σ_k perimeter ratios; c and ρ water specific heat and density; α_s convective coefficient.
In (2) Θ_t is the teeth radial-axial average temperature rise:

$$\Theta_t = \frac{1}{h_t}\cdot\int_0^{h_t}\left(\frac{1}{\ell}\cdot\int_0^{\ell}\vartheta_t(y,r)\cdot dy\right)\cdot dr \qquad (3)$$

The solution of eq. (2) is the thermal profile $\theta_{ws}(y)$:

$$\theta_{ws}(y) = \theta_{wsb}\cdot\exp(-y/\lambda_s)+\theta_{ws_\infty}\cdot(1-\exp(-y/\lambda_s)), \qquad (4)$$

where: $\lambda_s = (c\cdot\rho\cdot Q_s)/(\alpha_s\cdot p_s)$, (5)
is a characteristic length of the water flow in the slot;

$$\theta_{wsb} = \theta_{ws}(y=0) \quad \text{and} \qquad (6)$$

$$\theta_{ws_\infty} = \sigma_i\cdot\Theta_{ie}+\sigma_t\cdot\Theta_t+\sigma_y\cdot\Theta_{yi} \qquad (7)$$

are the temperature rises at the bottom slot channel input and the asymptotic output temperature rise respectively.
By integrating (2) along the lamination stack ℓ, some global equations are obtained, whose circuit interpretation is shown in fig.2: it includes a temperature rise controlled power source (modelling the power absorbed by the water flow, via the transconductance $G_{Qs} = c\cdot\rho\cdot Q_s$) and three power sources (portions of the teeth core losses P_{ft}). It should be noted that the circuit of fig.2 does not contain the variable Θ_t any more: in fact an expression of Θ_t has been substituted in (7), obtained from the thermal balance differential equation of the stator teeth (considering the specific core losses p_{ft} and the following thermal exchanges: teeth heads - gap water flow; teeth sides - slot water flow; teeth bases - internal stator yoke cylinder):

$$\Theta_t = \Theta_{tp}+\rho_t(\gamma_t)\cdot(\Theta_{ti}+\Theta_{yi}-2\cdot\Theta_{tp}), \qquad (8)$$

where

$$\Theta_{tp} = \Theta_{ws}+(p_{ft}\cdot b_t)/(2\cdot\alpha_s) = \Theta_{ws}+P_{ft}/(\sigma_t\cdot G_s)\,. \qquad (9)$$

As regards the other channels, analogous developments lead to obtain the water flow temperature rise profiles (similar to eq.(4)) and the related sub-networks; fig.3 refers to gap and notch channels: again, the transconductances model the thermal exchange with the water flow.
As can be noted, the sub-networks include just radial thermal phenomena, except for the water flow axial thermal exchanges, modelled by the controlled sources, whose power depends on the top-bottom $\Delta\theta$ differences.

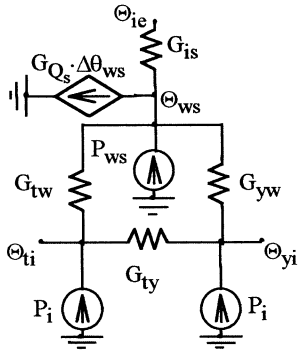

$$P_i = \rho_t(\gamma_t)\cdot P_{ft} \qquad (10)$$
$$P_{ws} = [1-2\cdot\rho_t(\gamma_t)]\cdot P_{ft} \qquad (11)$$
$$\rho_t(\gamma_t) = \frac{\cosh(\gamma_t)-1}{\gamma_t\cdot\sinh(\gamma_t)} \qquad (12)$$
$$\gamma_t = h_t/\lambda_t \qquad (13)$$
$$\lambda_t = \sqrt{\frac{k_\ell\cdot b_t}{2\cdot\alpha_s}} \qquad (14)$$

Fig.2. Slot channel equivalent sub-network and related quantities (k_ℓ is the iron thermal conductivity along the lamination).

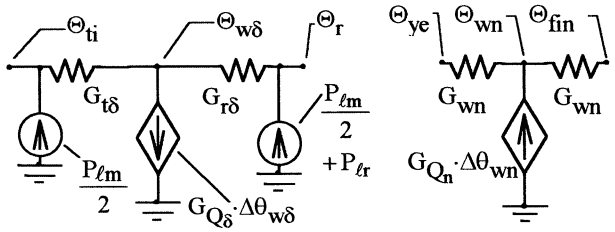

Fig.3. Gap (left) and notch (right) channels equivalent sub-networks ($P_{\ell m}$ and $P_{\ell r}$ are the friction and rotor Joule losses respectively).

B. Model of the stator winding

For the stator winding thermal model, we assume:
- the coil side is subdivided in: slot conductors (length ℓ), top and bottom half endwindings (length $\ell_e/2$ each);
- all the slot wires have the same thermal conditions;
- each copper wire cross section is assumed isothermal;
- the thermal flux in the insulation sheath is radial;
- y is extended along the wire axis: $-\ell_e/2 \le y \le \ell + \ell_e/2$.

Fig.4 shows an insulated wire portion, whose power balance referred to a slice of height dy is given by:

$$P_{in} - P_{out} = dP_{c\to w} - dP_J\,. \qquad (15)$$

By the Fourier's law, the difference $P_{in} - P_{out}$ becomes:

$$P_{in} - P_{out} = \frac{1}{r_\ell}\cdot\frac{d^2\theta_c(y)}{dy^2}\cdot dy\,, \qquad (16)$$

where $\theta_c(y)$ is the unknown temperature rise profile along the copper wire, and $r_\ell = 1/(k_c\cdot A_c)$ is the wire longitudinal specific thermal resistance (per unit length); k_c is the thermal Cu conductivity; A_c the wire cross section.

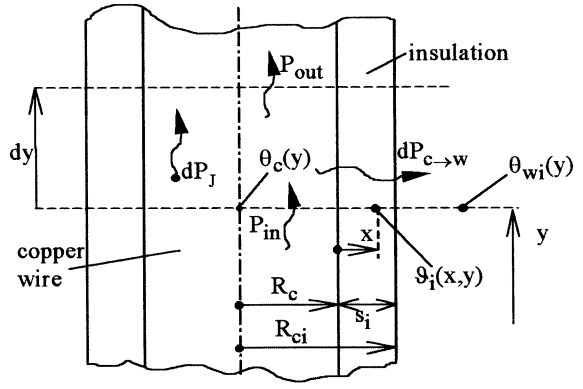

Fig. 4. Insulated wire segment and corresponding thermal powers.

The power developed in the elementary segment equals:

$$dP_J = p_J \cdot A_c \cdot dy \ , \quad (17)$$

with p_J specific loss in the stator winding [W/m^3]; the power flowing from the wire to the water equals:

$$dP_{c\to w} = g_t \cdot [\theta_c(y) - \theta_{wi}(y)] \cdot dy \ , \quad (18)$$

where g_t is the per unit length transversal thermal conductance among wire and water; g_t includes the insulation conductivity and the water convective factor α_i; in the slots $\alpha_i = \alpha_s$, while around the endwindings $\alpha_i = \alpha_e < \alpha_s$. Moreover, for the temperature rise $\theta_{wi}(y)$ we can write:

$$\begin{aligned} &-\ell_e/2 \le y < 0: && \theta_{wi}(y) = \theta_{wsb} \\ &0 \le y \le \ell: && \theta_{wi}(y) = \theta_{ws}(y) \\ &\ell < y \le \ell + \ell_e/2: && \theta_{wi}(y) = \theta_{wet} \end{aligned} \quad (19)$$

Thus, eq. (16) becomes:

$$\lambda_c^2 \cdot d^2\theta_c(y)/dy^2 - \theta_c(y) = -\theta_{wi}(y) - \lambda_c^2 \cdot p_J/k_c \ ; \quad (20)$$

$\lambda_c = 1/\sqrt{r_\ell \cdot g_t}$ is the insulated wire characteristic length.

Due to the different α_i values, it is opportune to solve eq. (20) separately in the three zones: in each part we have a solution of the associated homogeneous equation (with two integration constants), plus a particular solution ($\theta_{cpk}(y)$, with k = eb, s, et). By imposing suited conditions at the borders of each domain, we obtain [3]:

- bottom half endwinding wires ($-\ell_e/2 \le y \le 0$):

$$\theta_{ceb}(y) = \theta_{cpeb} + (\theta_{csb} - \theta_{cpeb}) \cdot \frac{\cosh\left(\frac{y + \ell_e/2}{\lambda_{ce}}\right)}{\cosh(\ell_e/(2 \cdot \lambda_{ce}))} \ , \quad (21)$$

$$\text{with } \theta_{cpeb} = \theta_{web} + \lambda_{ce}^2 \cdot p_J/k_c \ ; \quad (22)$$

- top half endwinding wires ($\ell \le y \le \ell + \ell_e/2$):

$$\theta_{cet}(y) = \theta_{cpet} + (\theta_{cst} - \theta_{cpet}) \cdot \frac{\cosh\left(\frac{\ell + \ell_e/2 - y}{\lambda_{ce}}\right)}{\cosh(\ell_e/(2 \cdot \lambda_{ce}))} \ , \quad (23)$$

$$\text{with } \theta_{cpet} = \theta_{wet} + \lambda_{ce}^2 \cdot p_J/k_c \ ; \quad (24)$$

- active wires in slots ($0 \le y \le \ell$):

$$\theta_{cs}(y) = \theta_{cps}(y) + [\theta_{cst} - \theta_{cps}(\ell)] \cdot \frac{\sinh(y/\lambda_{cs})}{\sinh(\ell/\lambda_{cs})} + [\theta_{csb} - \theta_{cps}(0)] \cdot \frac{\sinh((\ell - y)/\lambda_{cs})}{\sinh(\ell/\lambda_{cs})} \ , \quad (25)$$

$$\text{with } \theta_{cps}(y) = \theta_{ws\infty} + \lambda_{cs}^2 \cdot \frac{p_J}{k_c} - \frac{\theta_{ws\infty} - \theta_{wsb}}{1 - (\lambda_{cs}/\lambda_s)^2} \cdot e^{-y/\lambda_s} \quad (26)$$

By imposing the same border thermal fluxes, θ_{csb} and θ_{cst} can be evaluated; once defined $D_y = \partial/\partial y$ and:

$$T_e = \tanh((\ell_e/2)/\lambda_{ce}) \ , \quad \text{it follows} \quad (27)$$

$$\theta_{csb} = \frac{\lambda_{cs} \cdot T_e \cdot \theta_{cpeb} + \lambda_{ce} \cdot [\theta_{cps}(0) + \lambda_{cs} \cdot D_y\theta_{cps}(0)]}{\lambda_{ce} + \lambda_{cs} \cdot T_e} \quad (28)$$

$$\theta_{cst} = \frac{\lambda_{cs} \cdot T_e \cdot \theta_{cpet} + \lambda_{ce} \cdot [\theta_{cps}(\ell) - \lambda_{cs} \cdot D_y\theta_{cps}(\ell)]}{\lambda_{ce} + \lambda_{cs} \cdot T_e} \quad (29)$$

Inserting (28) and (29) in (21), (23), (25) allows to determine the temperature rise of every winding point, once known θ_{web}, $\theta_{ws\infty}$ and θ_{wet}.

The temperature rise θ_{cmax} of the top endwinding eye, particularly important because it is the hottest one, is:

$$\theta_{cmax} = \theta_{cpet} + \frac{\theta_{cps}(\ell) - \lambda_{cs} \cdot D_y\theta_{cps}(\ell) - \theta_{cpet}}{\cosh\left(\frac{\ell_e/2}{\lambda_{ce}}\right) + \frac{\lambda_{cs}}{\lambda_{ce}} \cdot \sinh\left(\frac{\ell_e/2}{\lambda_{ce}}\right)} \ . \quad (30)$$

As concerns the thermal stress of the insulation, it is possible to determine the temperature rise distribution $\vartheta_i(x,y)$ in a generic insulation point (see fig.4); again, considering the differential equation of the elementary thermal flow balance, by some manipulations one obtains [3]:

$$R_c \le x \le R_{ci}: \ \vartheta_i(x,y) = \theta_c(y) + \\ -[g_t/(2 \cdot \pi \cdot k_i)] \cdot [\theta_c(y) - \theta_{wi}(y)] \cdot \ell n(x/R_c) \ . \quad (31)$$

In order to get the equivalent sub-network of the stator slot winding portion, it is necessary to calculate the axial average value of each term of eq. (20), just along the active wire length ℓ: from this integration, it follows:

$$[D_y\theta_{cs}(\ell) - D_y\theta_{cs}(0)] \cdot \lambda_{cs}^2/\ell - \Theta_{cs} = \Theta_{ws} - p_J \cdot \lambda_{cs}^2/k_c \quad (32)$$

Thus, the difference among the axial average temperature rises of copper Θ_{cs} and water Θ_{ws} in slot equals:

$$\Theta_{cs} - \Theta_{ws} = (1 + \varepsilon_\theta) \cdot \lambda_{cs}^2 \cdot p_J/k_c \ , \quad (33)$$

$$\text{where } \varepsilon_\theta = [D_y\theta_{cs}(\ell) - D_y\theta_{cs}(0)] \cdot k_c/(p_J \cdot \ell). \quad (34)$$

Called P_{Js} the slot wire Joule losses, the following equation can be obtained [3], corresponding to the thermal sub-network of fig.5 (ε_θ is of the order of few percents):

$$\Theta_{cs} - \Theta_{ws} = R_{cs} \cdot P_{Js} \cdot (1 + \varepsilon_\theta) \approx R_{cs} \cdot P_{Js} \ . \quad (35)$$

The development of the field equations of the other machine portions (stator yoke, frame and machine-to-well thermal exchange interface), together with the corresponding expressions of the thermal profiles and sub-networks, are similar to the previously obtained ones.

III. SYNTHESIS OF THE THERMAL NETWORK

All the formerly developed sub-networks must be connected each other in order to obtain the global thermal network of the machine.

It should be noted that θ_{web}, $\theta_{ws\infty}$ and θ_{wet} of eq.s (22), (24), (26) are not known, as like as the differences $\Delta\theta$ controlling the dependent power sources: by some manipulations, all these variables can be expressed as a function of the temperature rises Θ at the sub-networks terminals. These nodal temperature rises (in the following called "cardinal") are unknown too, but their definition follows from the solution of the global thermal network.

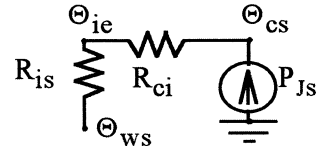

Fig. 5. Sub-network of the coil wires in the stator slots.

Subsequently, the evaluation of the cardinal temperature rises allows to obtain the axial temperature rises and the temperature rise profiles within each machine portion.
The global thermal network is shown in fig.6: the description of the nodes and of the independent and controlled sources is reported in Table I.

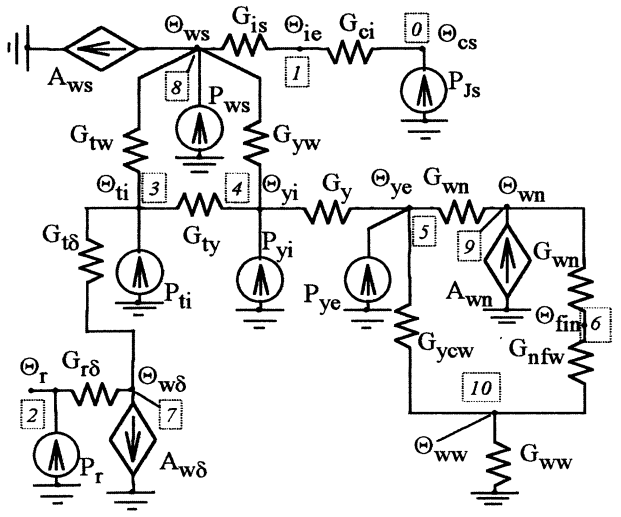

Fig.6. Global thermal network of the water cooled induction motor.

Table I – Main parameters of the global thermal network of fig.6: all the temperature rises are referred to the input well temperature (≡ 0)
Θ_k = axial average temperature rise in the cardinal node "k"

description of the cardinal nodes	
node N° 0 (Θ_{cs}) =	active conductors in stator slots
node N° 1 (Θ_{ie}) =	external surface of the slot conductor insulation
node N° 2 (Θ_r) =	external surface of the rotor
node N° 3 (Θ_{ti}) =	stator teeth head surface (towards the gap)
node N° 4 (Θ_{yi}) =	stator yoke internal surface (≅ stator teeth base)
node N° 5 (Θ_{ye}) =	stator yoke external surface (towards the frame)
node N° 6 (Θ_{fin}) =	internal frame surface (towards the notch)
node N° 7 ($\Theta_{w\delta}$) =	axial average temp. rise of the water flow in the gap
node N° 8 (Θ_{ws}) =	axial ave. temp. rise of the water flow in the slots
node N° 9 (Θ_{wn}) =	axial ave. temp. rise of the water flow in the notches
node N° 10 (Θ_{ww}) =	water flow in the well, after the motor
description of the independent power sources	
P_{Js} = joule power losses of the stator winding conductors in slots	
P_r = losses injected in the rotor node (cage + half friction $P_{\ell m}$)	
P_{ti} = losses injected in the node N° 3 (P_i + half friction $P_{\ell m}$; see eq.(10))	
P_{yi} = losses injected in the node N° 4 (P_i + half yoke core losses)	
P_{ye} = losses injected in the node N° 5 (half yoke core losses)	
P_{ws} = losses injected in the node N° 8 (see eq.(11))	
description of the axial temperature rise differences	
$\Delta\theta_{we} = P_{Je}/G_{Qs}$: temperature rise due to the Joule endwinding losses	
$\Delta\theta_{w\delta} = \theta_{w\delta t} - \theta_{wb}$: temperature rise difference along the gap channel	
$\Delta\theta_{ws} = \theta_{wst} - \theta_{wsb} = \theta_{wet} - \theta_{wb} - 2\cdot\Delta\theta_{we}$: $\Delta\theta$ along the slot channel	
$\Delta\theta_{wn} = \theta_{wt} - \theta_{wb}$: temperature rise difference along the notch channel	
description of the controlled power sources of the cooling channels	
$A_{w\delta} = G_{Q\delta}\cdot\Delta\theta_{w\delta}$	power of the gap water (absorbed by the flow)
$A_{ws} = G_{Qs}\cdot\Delta\theta_{ws}$	power of the slot water (absorbed by the flow)
$A_{wn} = G_{Qn}\cdot\Delta\theta_{wn}$	power of the notch water (delivered by the flow)

IV. SIMULATION RESULTS

A. *Cardinal node temperature rises*

In the following, some simulation results regarding a two-pole motor operating in rated conditions are shown (f_n= 50 Hz, P_n= 30 kW; other machine data in [1]).
Table II shows the axial and radial temperature rises obtained by solving the network of fig.6: reference is made to the nodes considered in fig.s 1 and 6 and to Table I.
About network structure and results, it can be noted that:
- the independent power sources include mixed contributions (portions of Joule, friction, core losses,...): this is the consequence of the sub-networks development, that leads to suitably concentrate the losses in the terminals;
- in the network of fig.6 just the loss terms included within the lamination stack are evidenced: in particular P_{Js} include just the stator Joule losses in the slots; conversely, the endwinding losses are taken into account in the power balance equations concerning the water flows in the bottom and top chambers (see $\Delta\theta_{we}$ in Table I);
- the temperature rise values appear not particularly high compared with those of standard air-cooled machines: this is the consequence of using PVC as insulation material for the winding: in fact, it presents a good non-hygroscopic behaviour in presence of water, but it does not allow to reach higher temperature levels.

Table II – Temperature rise values of the cardinal nodes of the network of fig.6 and Table I and axial temperature rises of fig.1 [K] (temperature rises are referred to the well water temperature before the motor).

stator slot active conductors: Θ_{cs}	25.4
insulation external surface in slot: Θ_{ie}	22.6
rotor external surface: Θ_r	34.1
stator teeth head node (towards the gap): Θ_{ti}	33.5
stator yoke internal node (≅ stator teeth base): Θ_{yi}	12.5
stator yoke external node (towards the frame): Θ_{ye}	6.9
internal frame surface (towards the notch): Θ_{fin}	2.0
water flow in the gap: $\Theta_{w\delta}$	33.8
water flow in the slots: Θ_{ws}	17.7
water flow in the notches: Θ_{wn}	14.5
water flow in the well (after the motor): Θ_{ww}	0.04
external frame surface (in front of the notches): Θ_{fen}	1.1
internal frame surface (at the contact with the yoke): Θ_{fic}	3.4
external frame surface (at the contact with the yoke): Θ_{fec}	1.9
bottom chamber water: θ_{wb} ($=\theta_{w\delta b}=\theta_{wnb}$)	8.7
gap water, top: $\theta_{w\delta t}$	34.0
slot water, bottom: θ_{wsb}	10.6
slot water, top: θ_{wst}	20.7
slot output water, after top endwindings: θ_{wet}	22.7
top chamber water: θ_{wt} ($=\theta_{wnt}$)	24.2

B. Temperature rise profiles in machine portions

The values of Table II allow to calculate the unknown terms in the thermal field solutions, leading to reconstruct the temperature profiles within each motor portion.
In fig.7 the core temperature rise profile along the radial direction is shown, together with the axial average temperature rises of the slot wires and of the water flows in the three channels. The following remarks can be made:
- the temperature rises of rotor, gap water and stator teeth heads are very close: this testifies the high level of the convective coefficient, dependent on the rotor speed;
- the radial temperature rise along the teeth is greatly decreasing, thanks to the convective cooling effect of the slot water flow and to the thermal conduction towards the stator yoke: the average temperature rise of the slot water flow is lower than that of slot wires and teeth;
- the radial temperature rise across the stator yoke decreases when approaching the external diameter, thanks to the cooling effect of the water flowing in the notches.

As regards the axial profiles, fig.8 shows that of the water flow in the gap, while fig.9 illustrates the profiles of the water flows in the slot and in the notch channels.
The peculiarity of the temperature rise profile of the water in the gap is that it reaches almost immediately the asymptotic value (in spatial sense), that is very close to the average axial value $\Theta_{w\delta}$: this effect is due to the very low value of the characteristic length (λ_δ), thanks to the high value of the convective coefficient in the gap (α_δ).

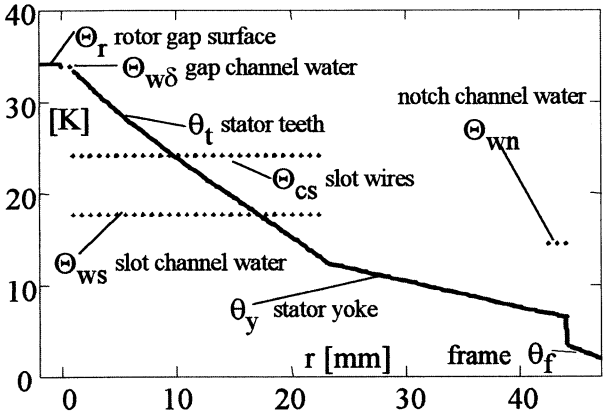

Fig.7. Radial distribution of the temperature rise in the motor:
..... axial average values (channels water, slot wires);
—— radial core profile, from rotor to frame
(r measured from the rotor surface).

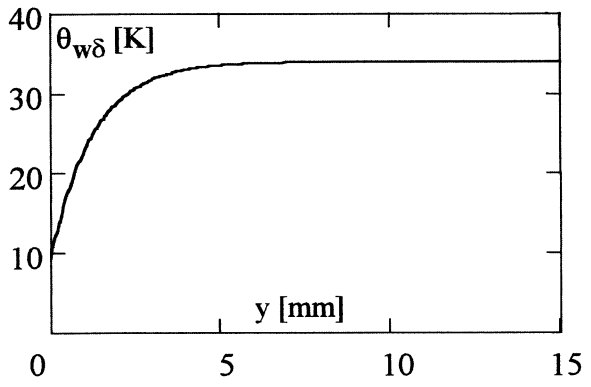

Fig.8 – Temperature rise profile of the water flow in the gap channel.

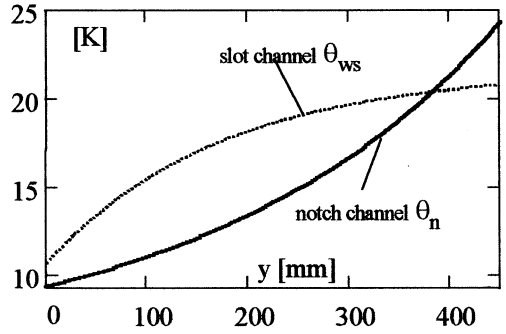

Fig.9. Water flow temperature rise profile in slot and notch channels.

On the other hand, the water in the slot channel, even if sensibly warming during its rising, reaches the top mixing chamber without arriving to the spatial steady-state asymptotic value, because of the lower convective coefficient in slot (α_s), whose effect is the higher value of the characteristic length ($\lambda_s = (c \cdot \rho \cdot Q_s)/(\alpha_s \cdot p_s)$).
The knowledge of the water temperature rise profile in the slot channel and around the endwindings (θ_{web}, θ_{wet}) allows to obtain the temperature rise profile of the winding $\theta_c(y)$, as shown in fig.10.
The temperature rises at the lamination stack edges are: θ_{csb} = 20.1 K, θ_{cst} =30.1 K; according to (30), the temperature rise of the hottest point is: $\theta_{c\,max}$ = 31.8 K.
Conversely, the minimum temperature rise, occurring in the bottom endwinding eye, is: $\theta_{c\,min}$ = 20.0 K .
The following remarks can be made:
- there are 6.4 K among the winding maximum temperature rise and the average copper temperature rise in slot: it is a difference that justifies the adoption of the field temperature model of the winding;
- there is a temperature gap of almost 12 K among the maximum and minimum winding temperature rise: it is a marked axial non-uniformity, corresponding to the warming of the water flow Q_s ($\Delta\theta_{ws} + \Delta\theta_{we}$ = 12.1 K);
- correspondingly, the temperature rise difference $\Delta\theta = \theta_c(y) - \theta_{wi}(y)$ appears roughly constant when considering different positions y along the winding.

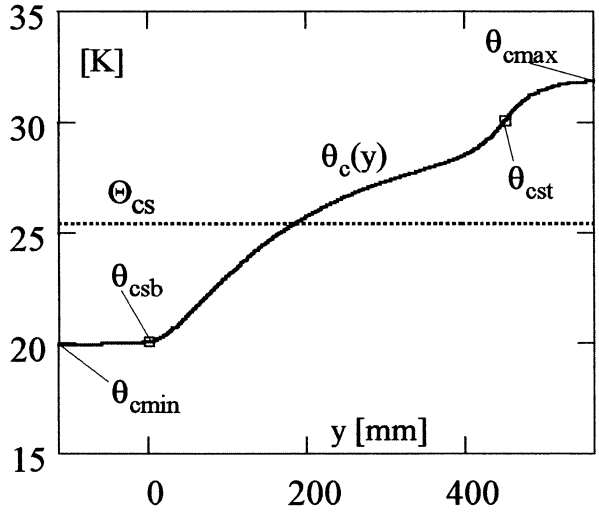

Fig.10. Temperature rise profile along the stator coil wires.

Fig.11 shows the temperature rise distribution in the insulation width, as a function of the generalised curvilinear co-ordinate y, measured along the winding wires axis:
- $\vartheta_i(y,\xi)$ is the temperature rise in the insulation, with ξ p.u. radial co-ordinate, measured from the copper wire surface and referred to the insulation width ($\xi = x/s_i$);
- $\vartheta_i(y,0) = \theta_c(y)$ is the copper wire temperature rise;
- $\theta_{wi}(y)$ is the water temperature rise near the insulation.

The following remarks can be made:
- the copper and insulation thermal profile is quite similar to that of the water around the wires;
- the effect of the local discontinuity of $\theta_{wi}(y)$ around the top end of the channel is reproduced mainly in the more external parts of the insulation width, while it appears sensibly smoothed in the $\theta_c(y)$ profile: this is due to the good thermal co-operation of the copper wires, that operates a re-distribution of the external thermal gradients;
- the theoretical logarithmic dependence of ϑ_i on ξ (see eq. (31)) is linear in practice, given the shortness of the thermal branch, equal to the insulation width s_i;
- the local minima of the insulation temperature rise near $y = 0$ depend on the local thermal exchange coefficient α_i: for $y < 0$, a constant value of θ_{wi} has been considered (equal to θ_{web}); correspondingly, also the shape of $\vartheta_i(y,\xi=1)$ is roughly constant, at least until also α_i remains constant at the value $\alpha_e < \alpha_s$; conversely, when approaching the slot input ($y = 0$), the water flow is accelerated, because a section contraction occurs: this increased speed of the water flow around the insulation increases α_i from α_e to α_s: this local improvement of α_i, being equal θ_{wi} in the vicinity, implies a local reduction of the external insulation temperature rise;
- the hollow of $\vartheta_i(0,\xi)$ near the local minima, maximum for $\xi = 1$, becomes weaker in the more internal zones of the insulation, and it disappears on the copper surface: also this effect is due to the thermal co-operation of the copper, thanks to its high conductivity;
- it is confirmed that the most stressed insulation point is that with temperature rise $\vartheta_i(y=\ell+\ell_e, \xi=0)$, that coincides with that of the hottest winding point (θ_{cmax}).

V. CONCLUSIONS

The paper presented a field-circuit analytical approach for the thermal analysis of water-cooled induction motors. The described procedure operates as follows:
- the motor is subdivided in thermal portions that can be homogeneously modelled;
- for each subsystem the temperature rise field solution and the equivalent thermal sub-network are obtained;
- linking the sub-networks gives the global thermal network, whose nodal unknown are temperature rises of internal parts and at the channels ends (cardinal nodes);
- once known the cardinal values, the most critical temperature rises can be evaluated; in particular:
  - top endwinding eye (hot spot);
  - output sections of the channels (where the water temperature must be well lower than the boiling limit).

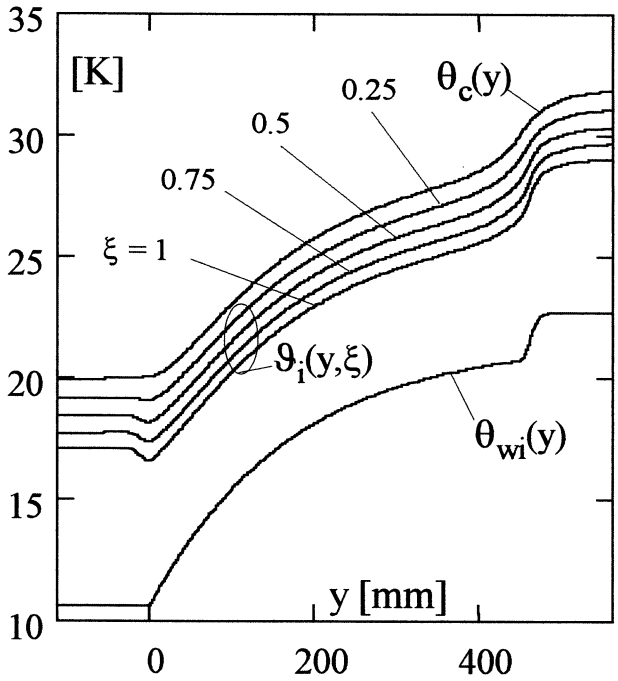

Fig. 11. Temperature rise profiles along each stator wire:
$\vartheta_i(y,\xi)$ = insulation temperature rise (ξ radial co-ordinate, in p.u., measured from the copper wire surface and referred to the insulation width);
$\theta_c(y)$ = copper wire temperature rise;
$\theta_{wi}(y)$ = temperature rise of the water near the insulation.

The values of the temperature rises and the thermal profiles in the different portions of the machines appear reasonable and congruent with some measured values of preliminary tests, also for operating conditions different from the described one.
Possible future method improvements will include:
- thermal model refinements, both in terms of network topological structure and as regards the estimation of the thermal exchange parameters;
- channel fluid-dynamical circuit modelling;
- use of the developed model in order to verify the optimisation level of the internal cooling system;
- experimental tests on instrumented machines.

VI. REFERENCES

[1] A. Di Gerlando, R. Perini, I. Vistoli, G. Bosi, "Design and Operation Improvements of Inverter Fed Adjustable Speed Induction Motors for Pumping Applications", *Proceedings of ICEM'96*, Vigo, Spain, Sept. 1996, pp.236-241.

[2] A. Di Gerlando, R. Perini, I. Vistoli, "Modelling and Design Aspects of Inverter Fed Solid Rotor Submersible Induction Motors for Pumping Drives", *Proceedings of ICEM'98*, Istanbul, Turkey, Sept. 1998, pp.1461-1467.

[3] A. Di Gerlando, R. Perini: "Analytical evaluation of the stator winding temperature field of water-cooled induction motors for pumping drives", *Proceedings of ICEM'00*, Espoo, Finland, Aug. 2000, pp.130-134.